Electronic Supplementary Material (ESI) for Journal of Materials Chemistry A.

Supporting Information for

Improving areal capacity of flexible Li–CO_2 batteries by constructing freestanding cathode with monodispersed MnO nanoparticles in N-doped mesoporous carbon nanofibers

Siwu Li, Yuan Liu, Xing Gao, Jiaming Wang, Junwen Zhou, Lu Wang,* and Bo Wang*

Beijing Key Laboratory of Photoelectronic/Electrophotonic Conversion Materials, Key Laboratory of Cluster Science, Ministry of Education, School of Chemistry and Chemical Engineering, Beijing Institute of Technology Beijing 100081, P. R. China

E-mail: bowang@bit.edu.cn, luwang@bit.edu.cn

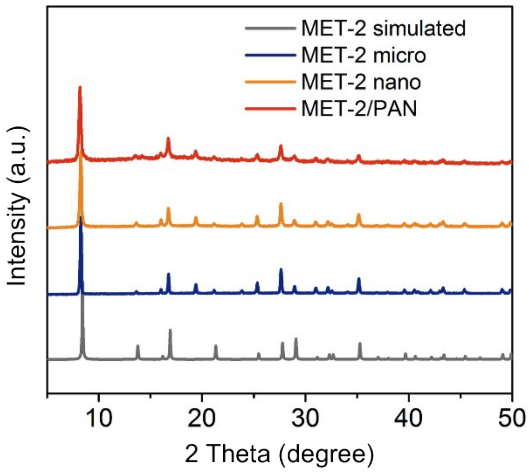

Fig. S1 PXRD patterns of different types of MET-2 particles and their PAN composite.

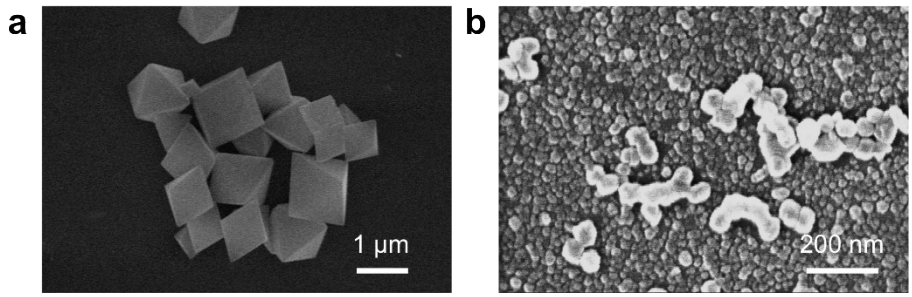

Fig. S2 SEM images of (a) mirco-sized MET-2 and (b) nano-sized MET-2 particles.

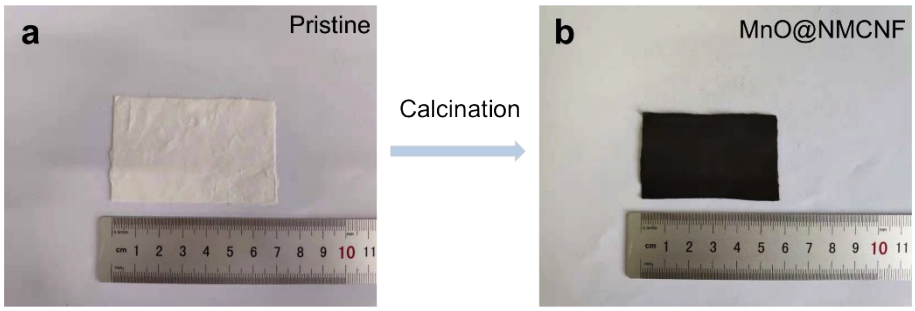

Fig. S3 Photos of (a) pristine MET-2/PAN film and (b) its corresponding product after calcination at 800 °C.

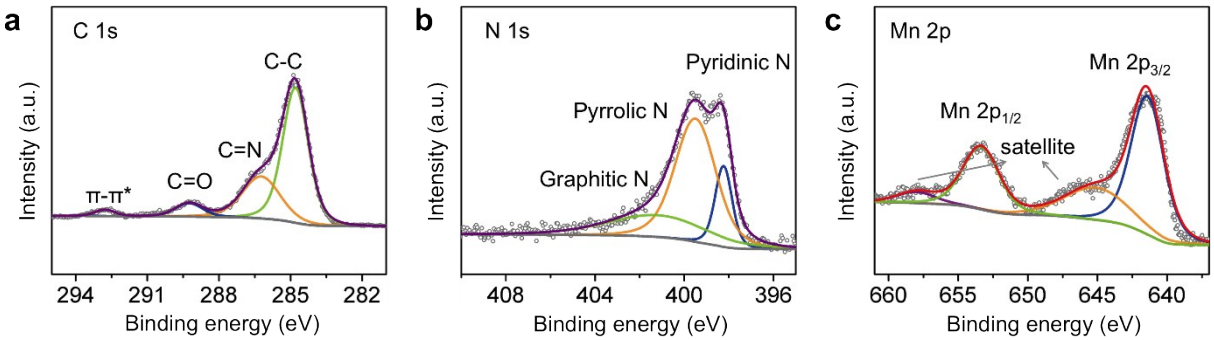

Fig. S4 XPS spectra of (a) C 1s, (b) N 1s and (c) Mn 2p for MnO@NMCNF.

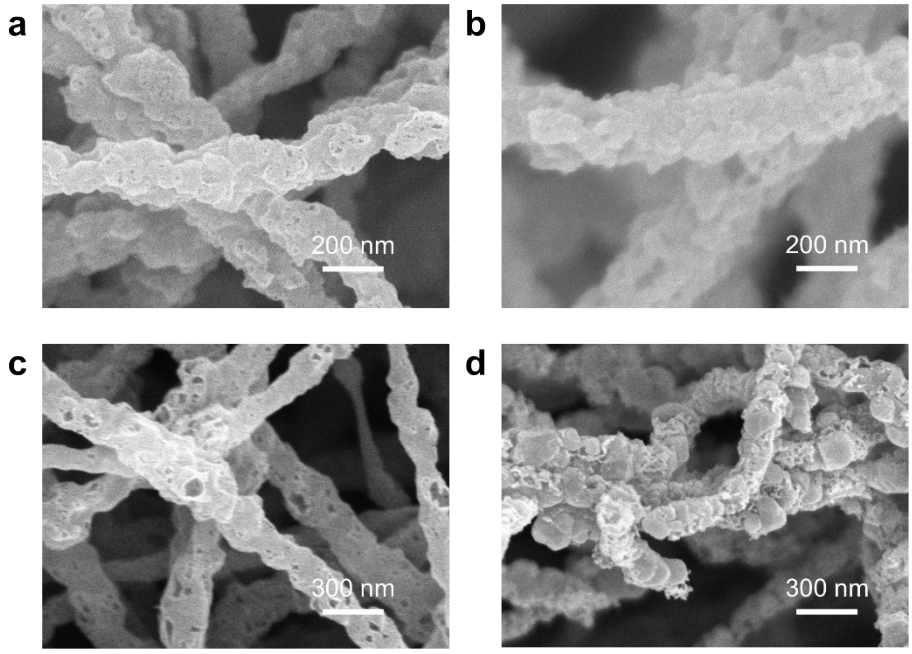

Fig. S5 SEM images of (a) MnO@NMCNF-600, (b) MnO@NMCNF-700, (c) MnO@NMCNF and (d) MnO@NMCNF-900.

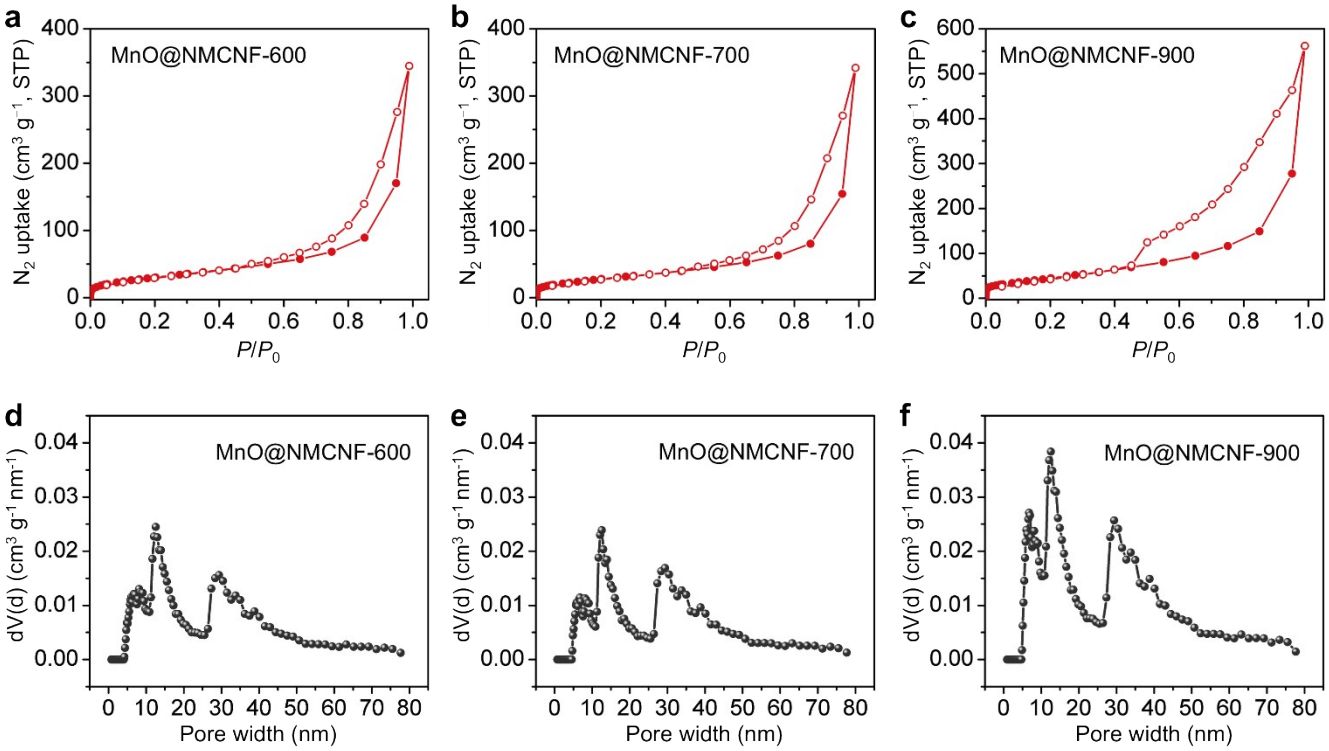

Fig. S6 N_2-77 K adsorption isotherms of (a) MnO@NMCNF-600, (b) MnO@NMCNF-700 and (c) MnO@NMCNF-900 and (d-f) corresponding pore distribution.

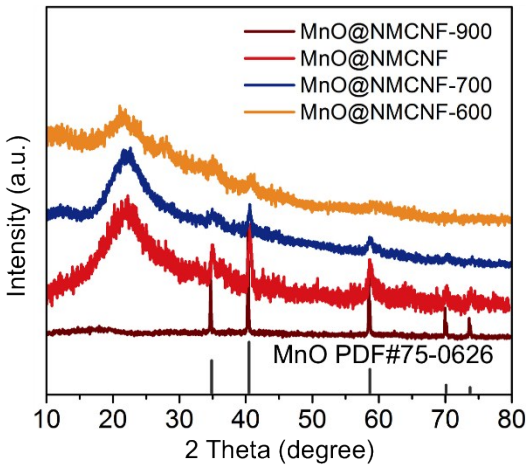

Fig. S7 PXRD patterns of MET-2/PAN (with MOF ratio of 60 wt%) fibers calcined at different temperatures.

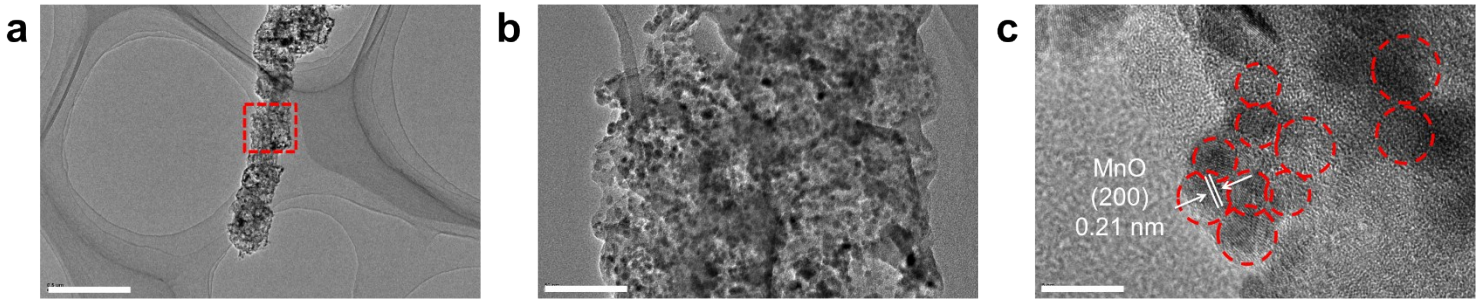

Fig. S8 (a, b) TEM and (c) HRTEM images of MnO@NMCNF-600. Scale bar: 500 nm in (a), 50 nm in (b), 5 nm in (c).

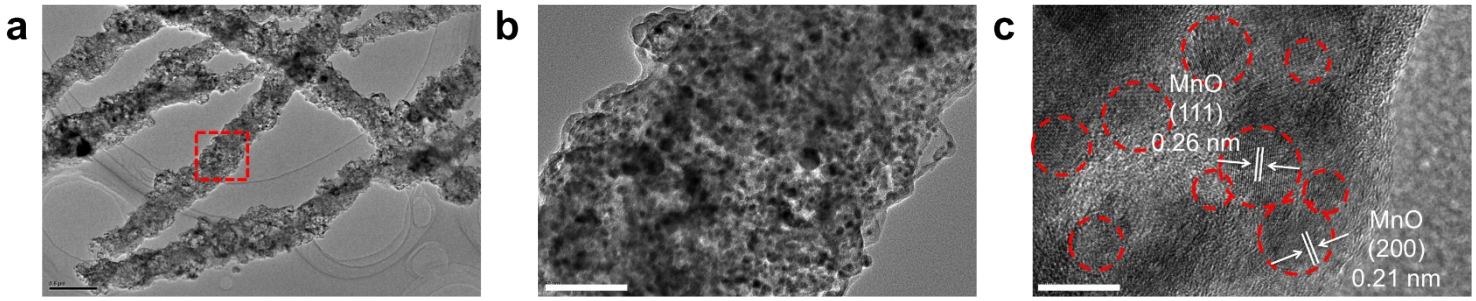

Fig. S9 (a, b) TEM and (c) HRTEM images of MnO@NMCNF-700. Scale bar: 500 nm in (a), 50 nm in (b), 5 nm in (c).

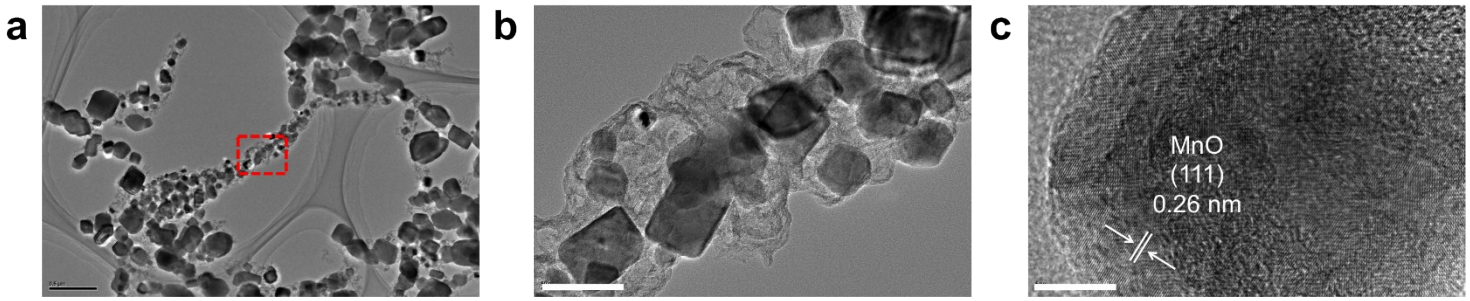

Fig. S10 (a, b) TEM and (c) HRTEM images of MnO@NMCNF-900. Scale bar: 500 nm in (a), 50 nm in (b), 5 nm in (c).

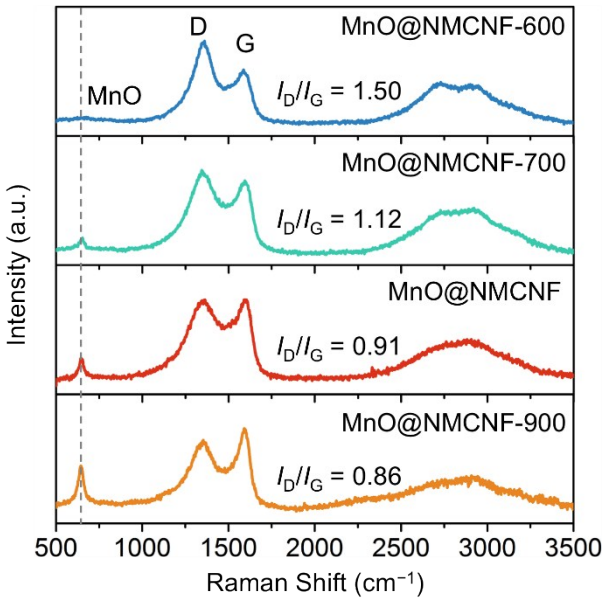

Fig. S11 Raman spectra of MnO@NMCNF-600, MnO@NMCNF-700, MnO@NMCNF and MnO@NMCNF-900.

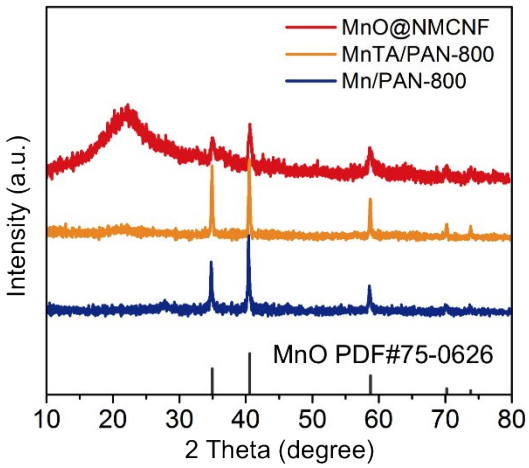

Fig. S12 PXRD patterns of different Mn-based fibers calcined at 800 °C.

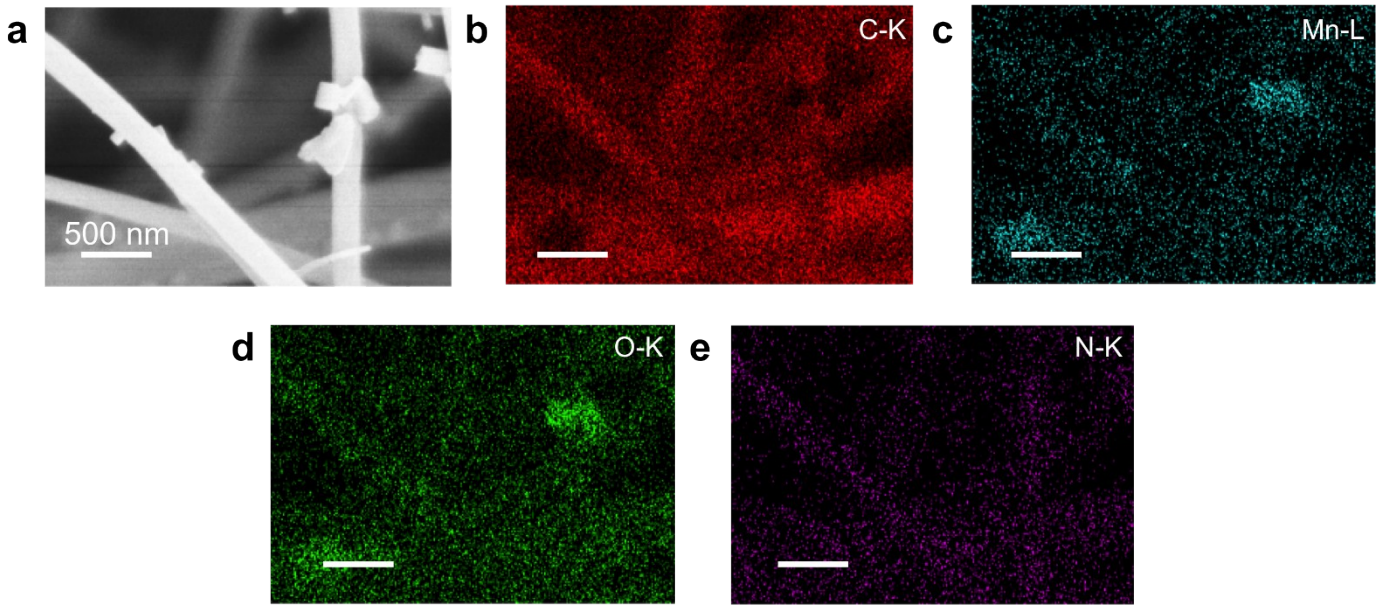

Fig. S13 (a) SEM image of Mn/PAN-800 and (b–e) corresponding elemental mappings of C, Mn, O and N. Scale bar: 500 nm in (b–e).

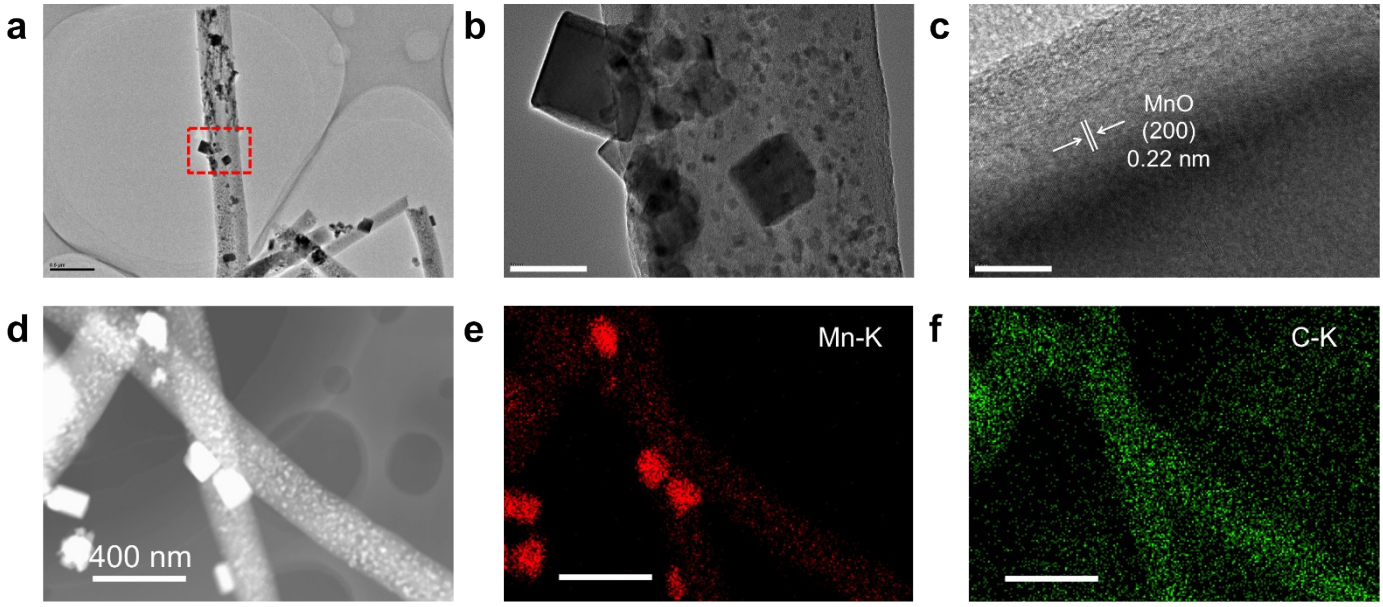

Fig. S14 (a, b) TEM and (c) HRTEM images of Mn/PAN-800. (d–f) STM image of Mn/PAN-800 and corresponding elemental mappings of Mn and C. Scale bar: 500 nm in (a), 50 nm in (b), 5 nm in (c), 400 nm in (e) and (f).

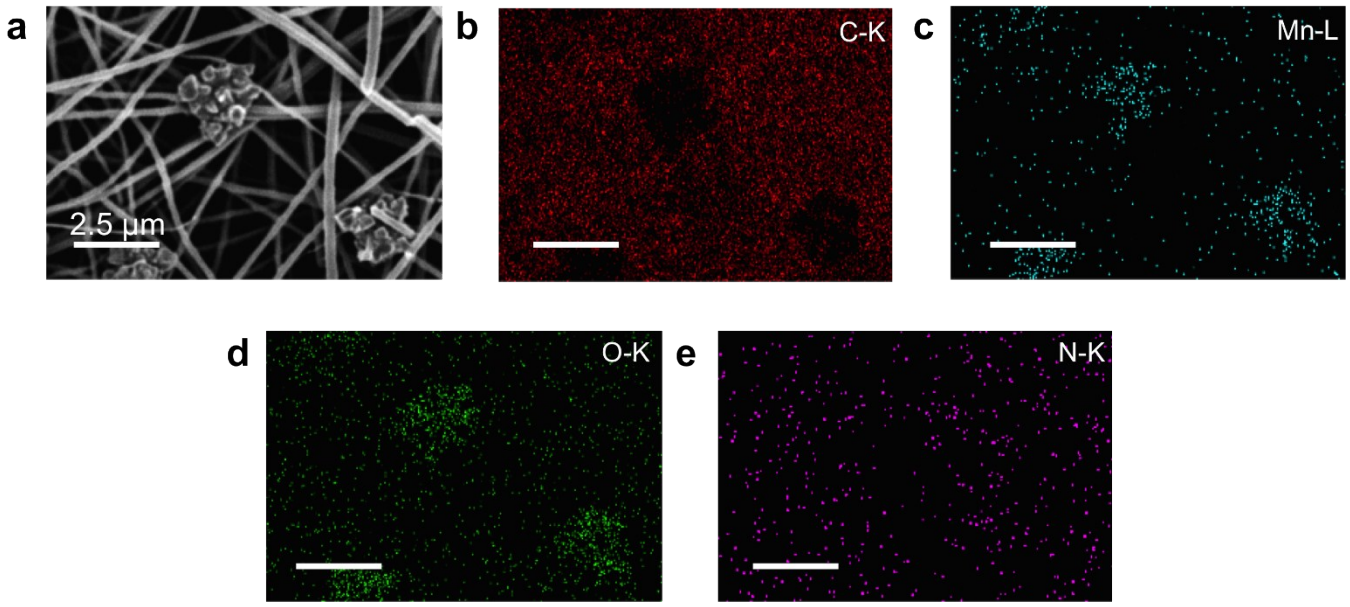

Fig. S15 (a) SEM image of MnTA/PAN-800 and (b–e) corresponding elemental mappings of C, Mn, O and N. Scale bar: 2.5 μm in (b–e).

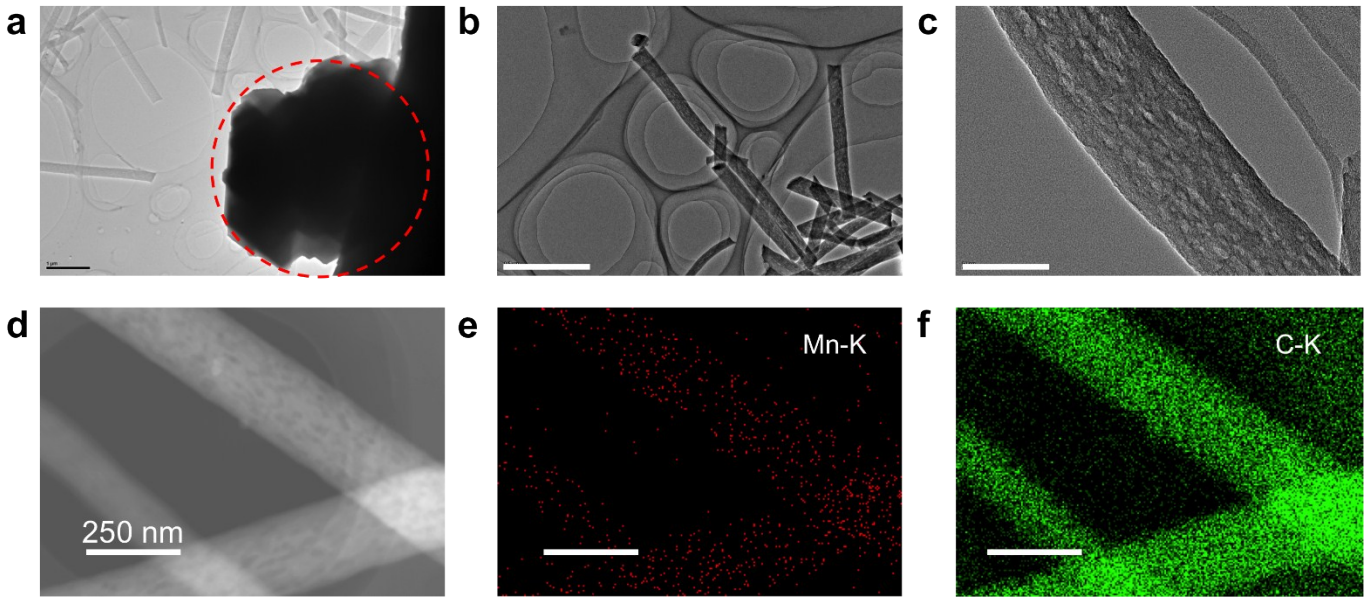

Fig. S16 (a, b) TEM and (c) HRTEM images of MnTA/PAN-800. (d–f) STM image of MnTA/PAN-800 and corresponding elemental mappings of Mn and C. Scale bar: 500 nm in (a), 50 nm in (b), 5 nm in (c), 250 nm in (e) and (f).

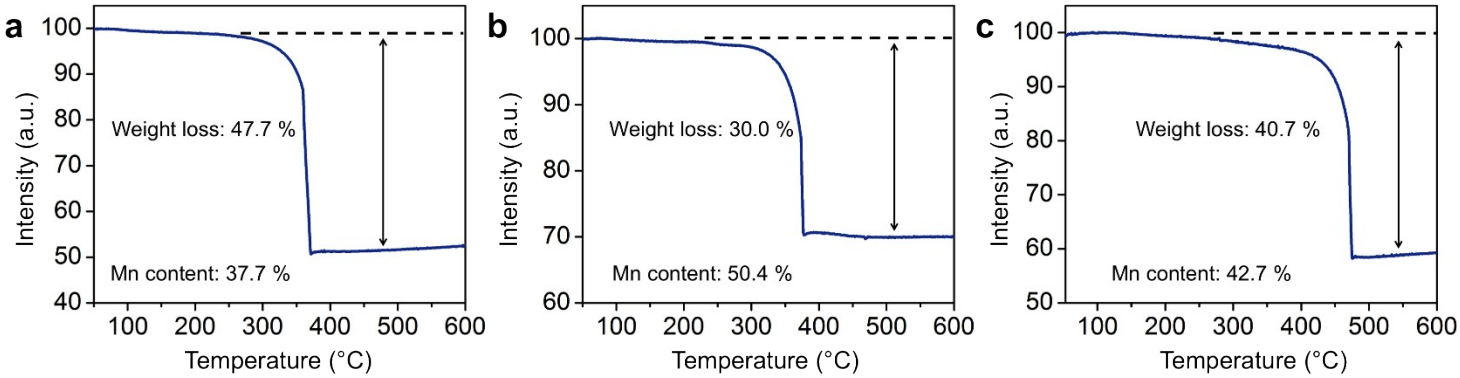

Fig. S17 TG curves of (a) MnO@NMCNF, (b) Mn/PAN-800 and (c) MnTA/PAN-800 tested under air atmosphere with a heating rate of 10 °C min^{-1}.

The weight ratio of Mn was calculated according to the PXRD result (Fig. S18) of their corresponding product after TG test.

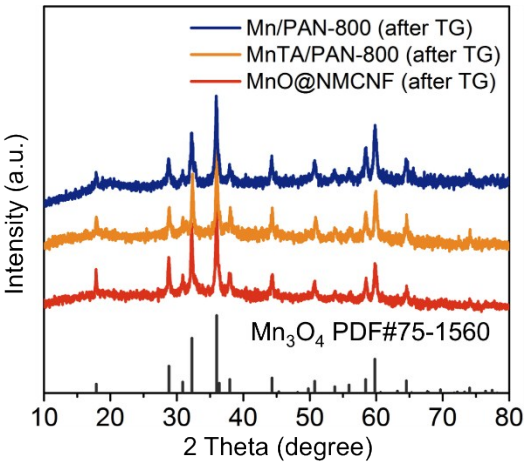

Fig. S18 PXRD patterns of the samples after TG test.

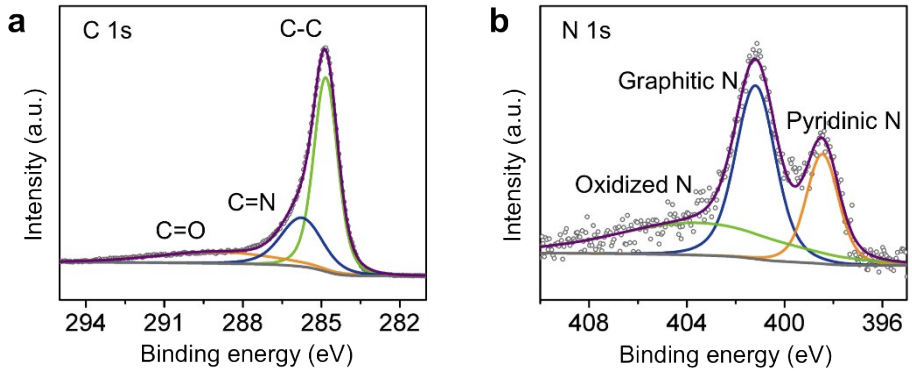

Fig. S19 XPS spectra of (a) C 1s and (b) N 1s for PAN-800.

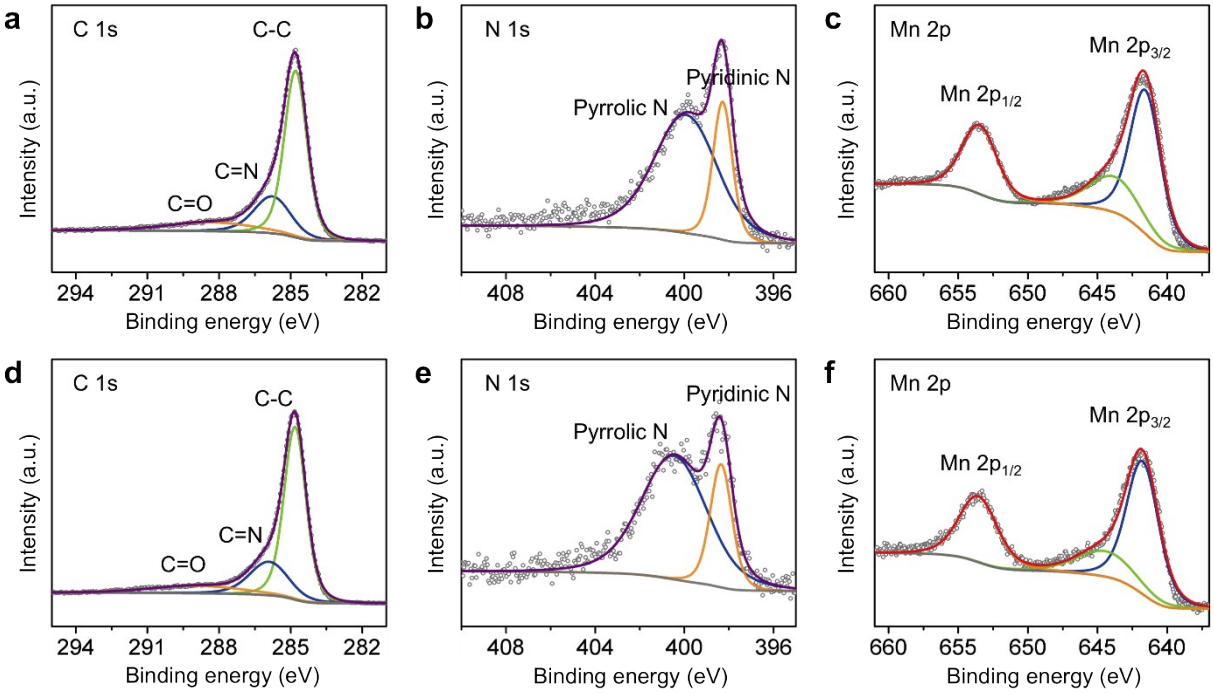

Fig. S20 XPS analysis of (a–c) Mn/PAN-800 and (d–f) MnTA/PAN-800.

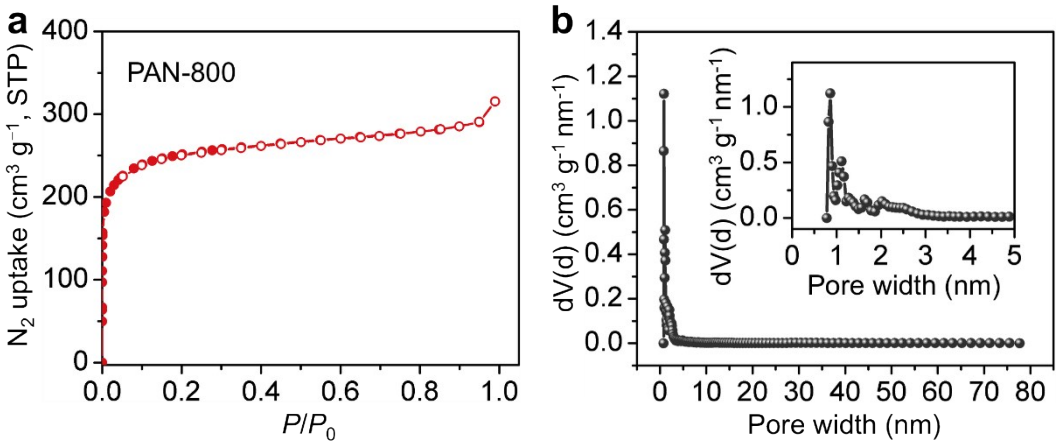

Fig. S21 (a) N_2-77 K adsorption isotherms of PAN-800. (b) Pore distribution of PAN-800 (inset shows a magnified plot with pore width within 0–5 nm).

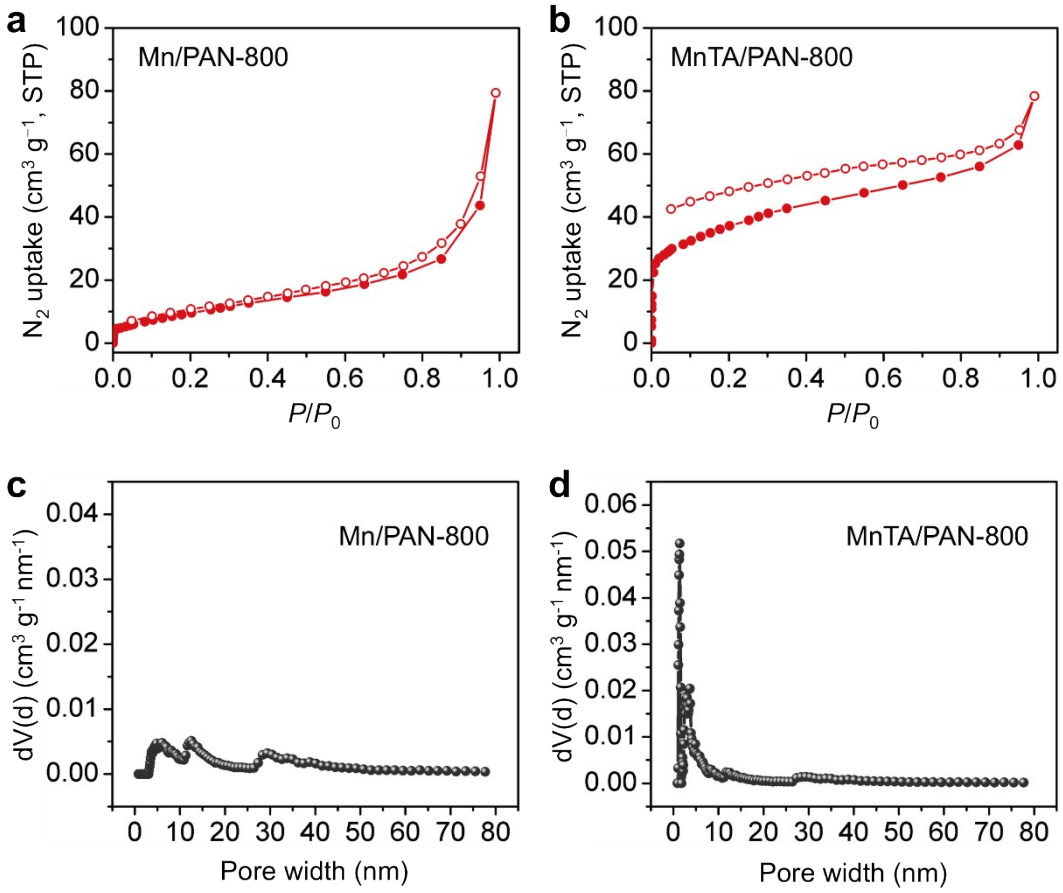

Fig. S22 N_2-77 K adsorption isotherms of (a) Mn/PAN-800 and (b) MnTA/PAN-800 and (c, d) corresponding pore distribution.

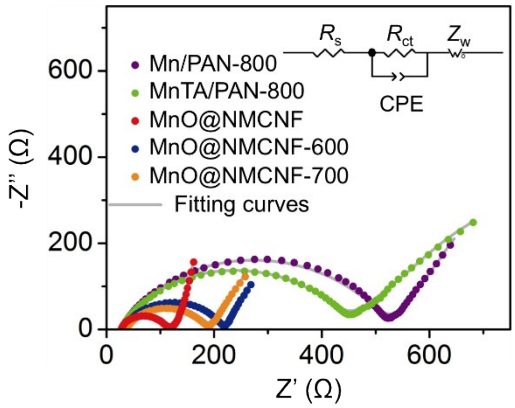

Fig. S23 Nyquist plots of Li–CO_2 cells with different Mn-based electrode materials before cycling (the inset is the equivalent circuit model for fitting the Nyquist plots).

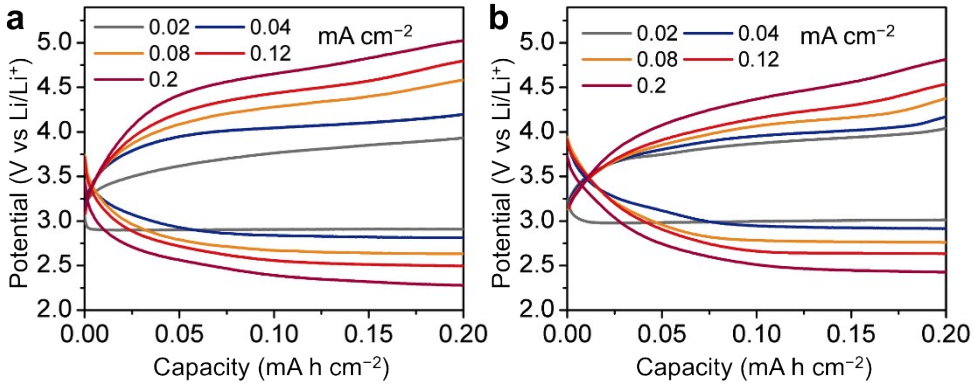

Fig. S24 Discharge-charge voltage curves of (a) MnO@NMCNF-600 and (b) MnO@NMCNF-700 at different current densities with a cut-off capacity of 0.20 mA h cm^{-2}.

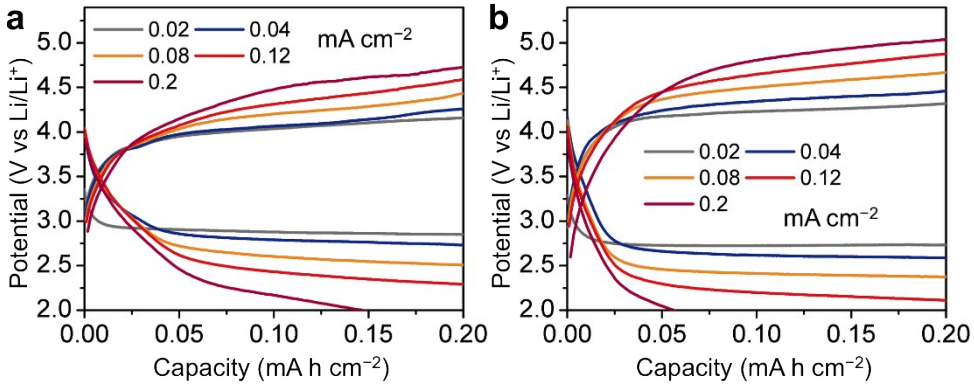

Fig. S25 Discharge-charge voltage curves of (a) Mn/PAN-800 and (b) MnTA/PAN-800 at different current densities with a cut-off capacity of 0.20 mA h cm^{-2}.

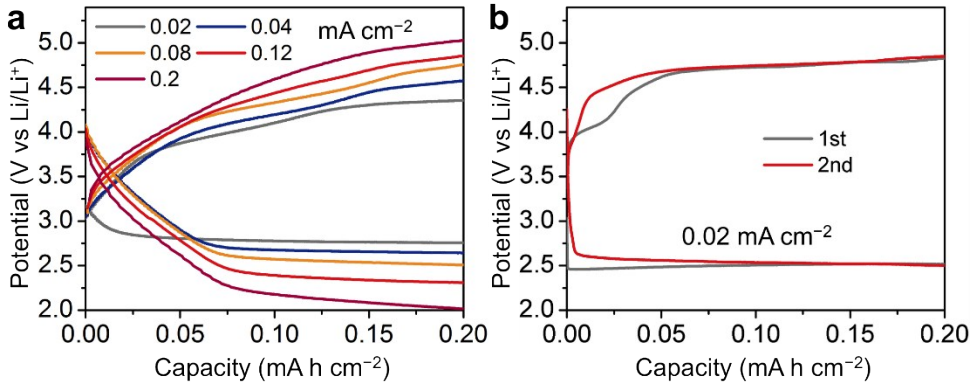

Fig. S26 Discharge-charge voltage curves of (a) PAN-800 and (b) carbon cloth at different current densities with a cut-off capacity of 0.20 mA h cm^{-2}.

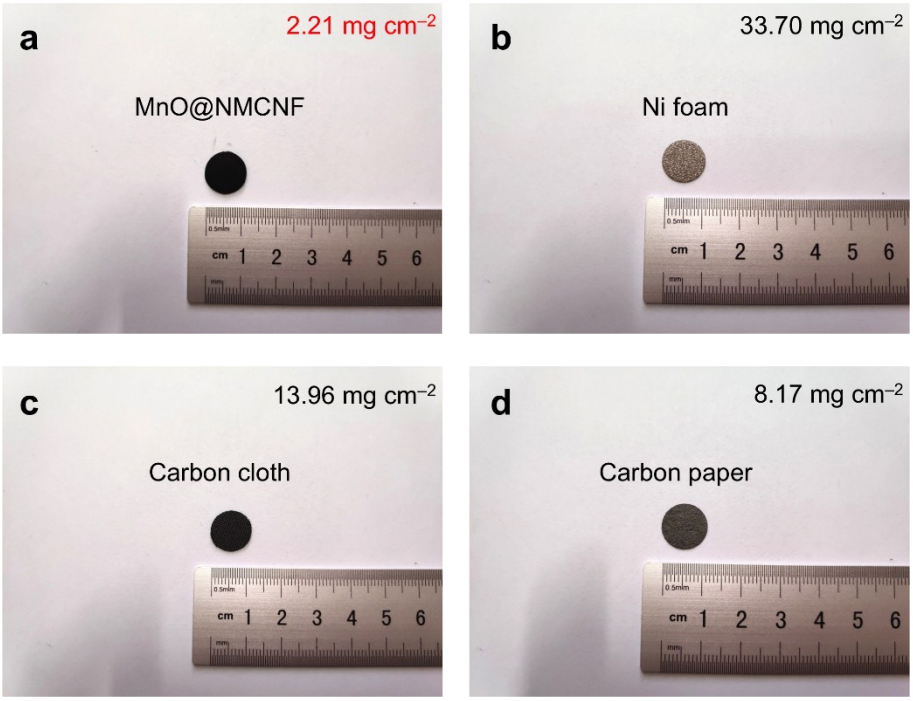

Fig. S27 Photos of different electrodes with diameter of 12 mm and their corresponding areal mass: (a) MnO@NMCNF, (b) Ni foam, (c) carbon cloth and (d) carbon paper.

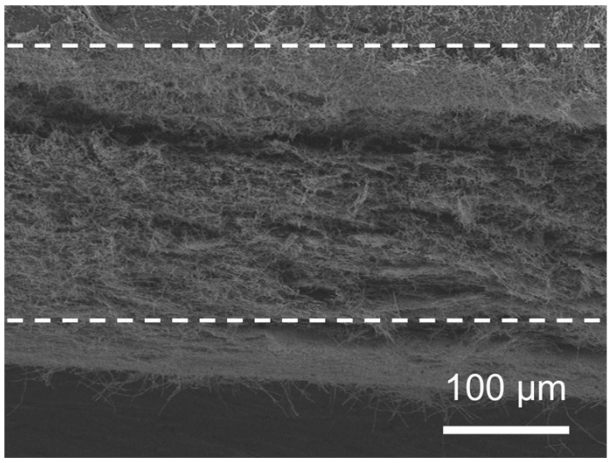

Fig. S28 SEM image of the cross-section of MnO@NMCNF.

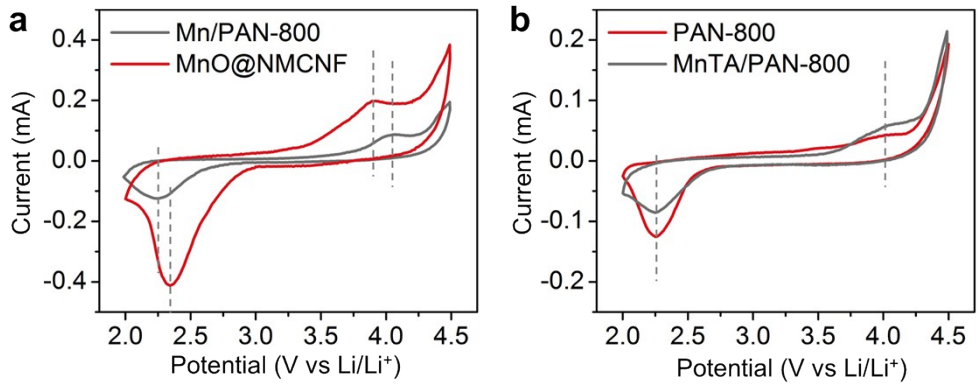

Fig. S29 Cyclic voltammetry curves of different Li–CO_2 cells at a scan rate of 0.1 mV s^{-1} with a voltage range of 2.0–4.5 V. (a) MnO@NMCNF and Mn/PAN-800. (b) PAN-800 and MnTA/PAN-800.

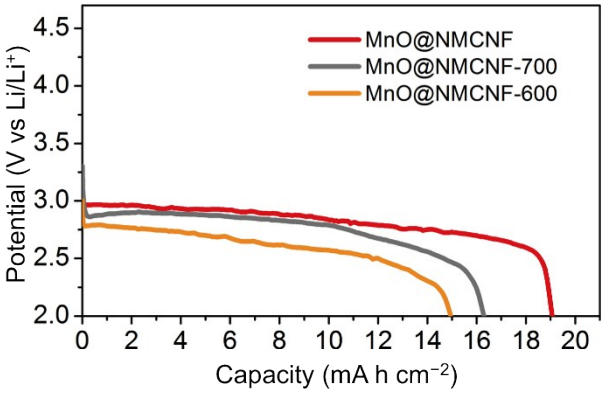

Fig. S30 Discharge profiles of MnO@NMCNF-600, MnO@NMCNF-700 and MnO@NMCNF cathodes at 0.04 mA cm^{-2} with a cut-off voltage of 2.0 V.

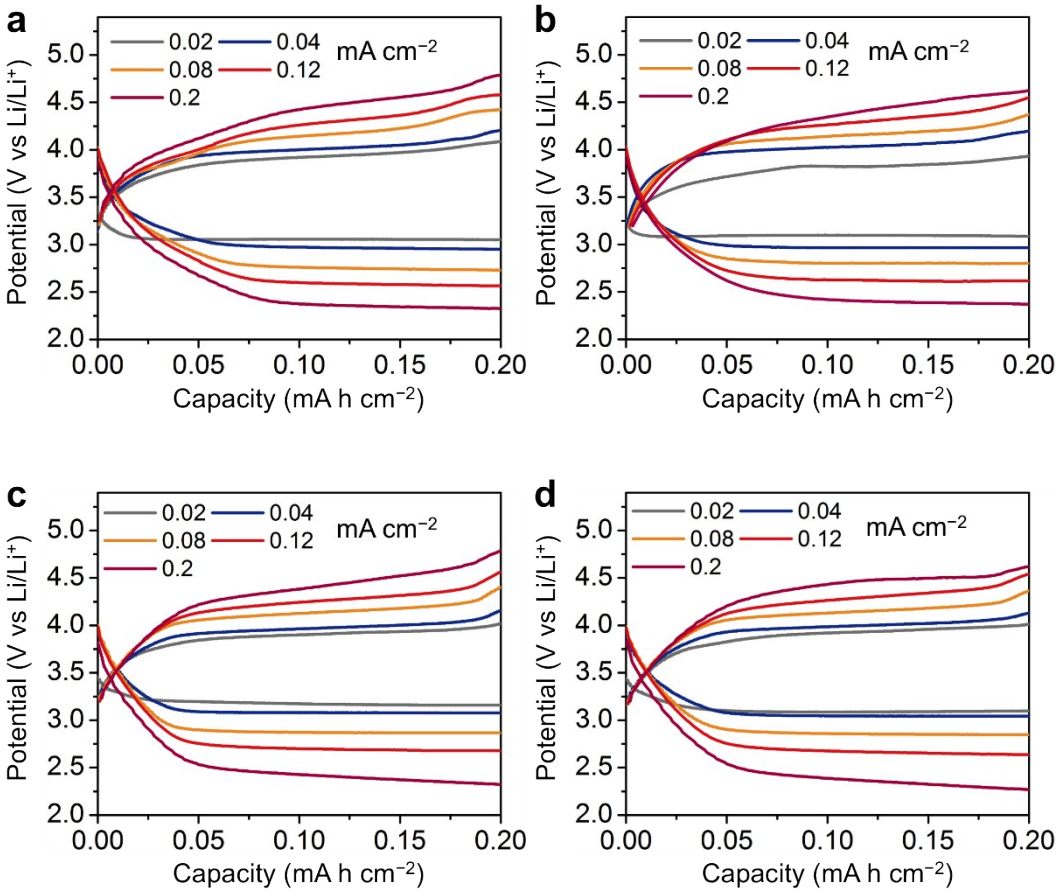

Fig. S31 Discharge-charge voltage curves of (a) MnO@NMCNF-R50, (b) MnO@NMCNF, (c) MnO@NMCNF-R70 and (d) MnO@NMCNF-R80 at different current densities with a cut-off capacity of 0.2 mA h cm^{-2}.

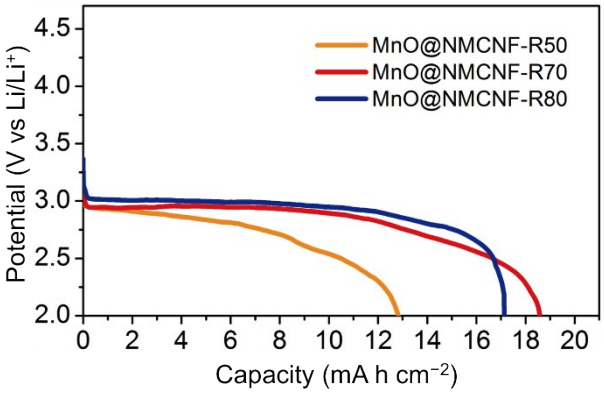

Fig. S32 Discharge profiles of MnO@NMCNF-R50, MnO@NMCNF-R70 and MnO@NMCNF-R80 cathodes at 0.04 mA cm^{-2} with a cut-off voltage of 2.0 V.

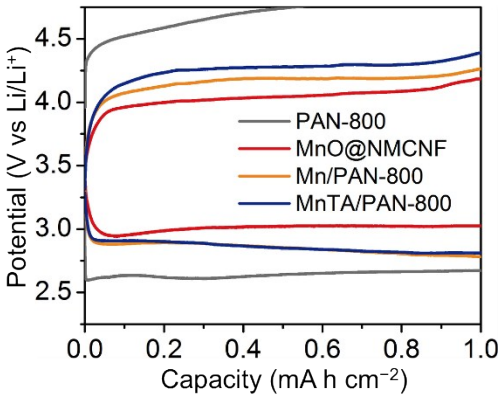

Fig. S33 Discharge-charge voltage curves of MnO@NMCNF, Mn/PAN-800, MnTA/PAN-800 and PAN-800 at 0.04 mA cm^{-2} with a cut-off capacity of 1 mA h cm^{-2}.

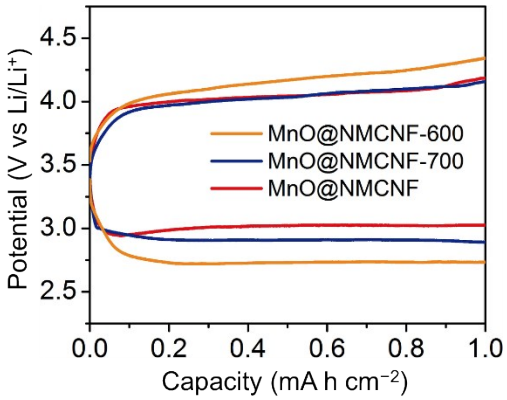

Fig. S34 Discharge-charge voltage curves of MnO@NMCNF-600, MnO@NMCNF-700 and MnO@NMCNF at 0.04 mA cm^{-2} with a cut-off capacity of 1 mA h cm^{-2}.

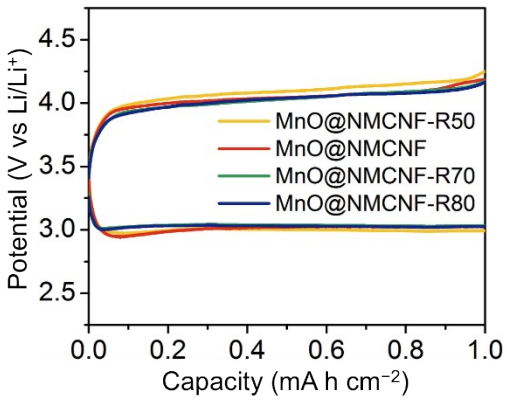

Fig. S35 Discharge-charge voltage curves of MnO@NMCNF-R50, MnO@NMCNF, MnO@NMCNF-R70 and MnO@NMCNF-R80 at 0.04 mA cm^{-2} with a cut-off capacity of 1 mA h cm^{-2}.

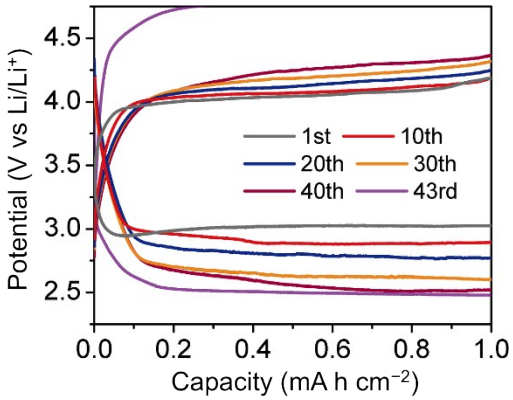

Fig. S36 Cycling performance of MnO@NMCNF at 0.04 mA cm^{-2} with a cut-off capacity of 1 mA h cm^{-2}.

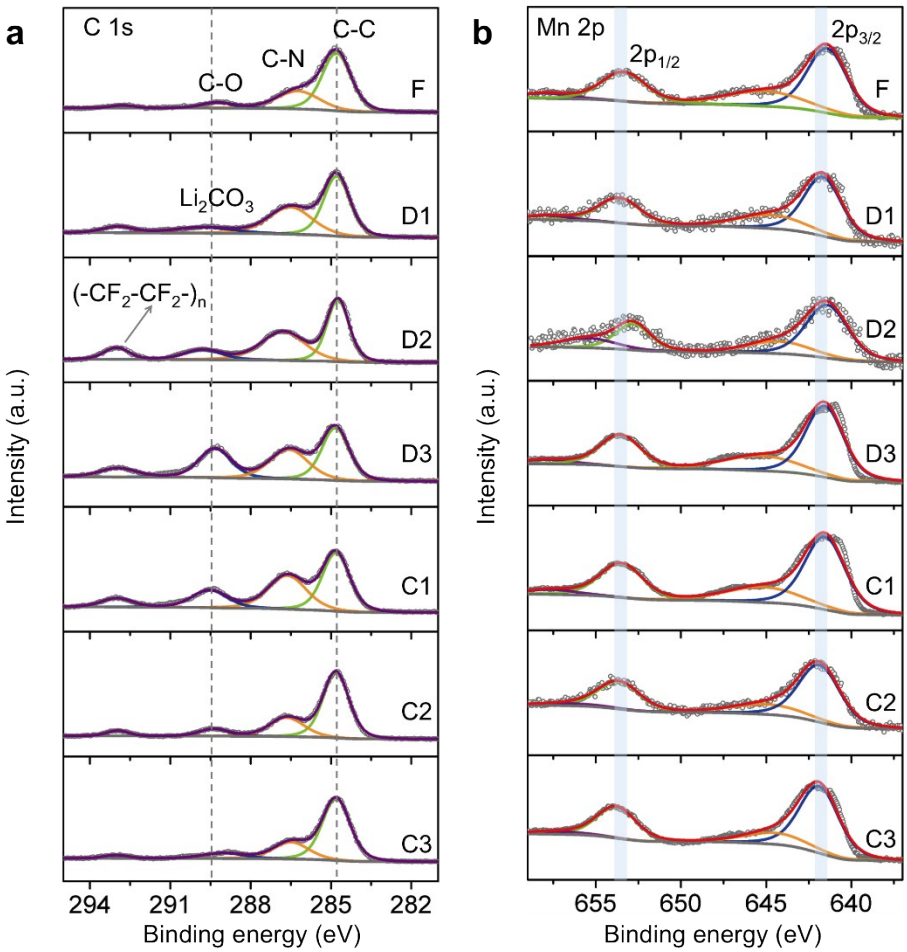

Fig. S37 XPS analysis of MnO@NMCNF electrodes at different states during operation at 0.04 mA cm^{-2} (F: fresh electrode; D1–D3: discharge to 0.2, 0.5 and 1 mA h cm^{-2}, respectively; C1–C3: recharged to 0.2, 0.5 and 1 mA h cm^{-2}, respectively): (a) C 1s and (b) Mn 2p spectra.

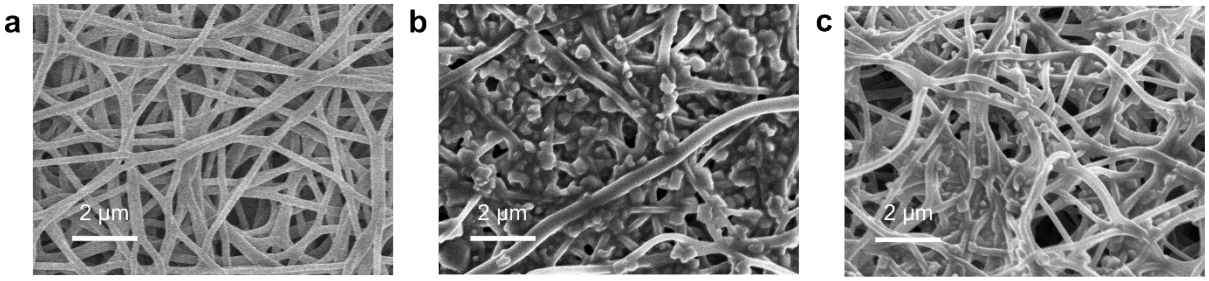

Fig. S38 SEM images of (a) a fresh, (b) a discharged and (c) a recharged PAN-800 cathode tested under 0.04 mA cm^{-2} with a cut-off capacity of 1.0 mA h cm^{-2}.

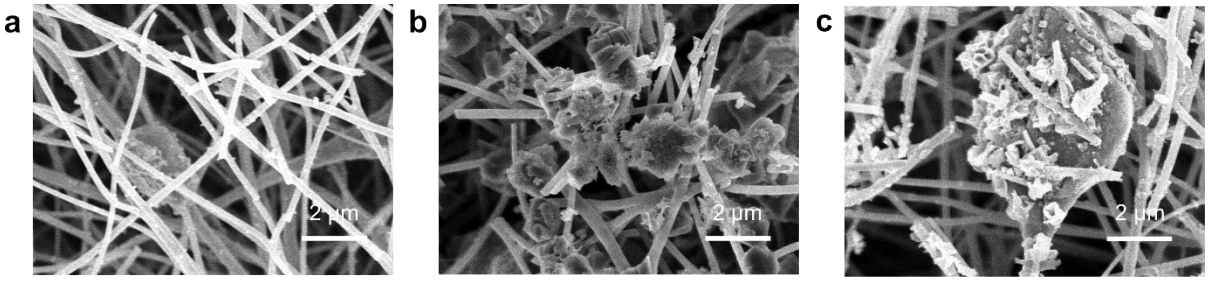

Fig. S39 SEM images of (a) a fresh, (b) a discharged and (c) a recharged Mn/PAN-800 cathode tested under 0.04 mA cm^{-2} with a cut-off capacity of 1.0 mA h cm^{-2}.

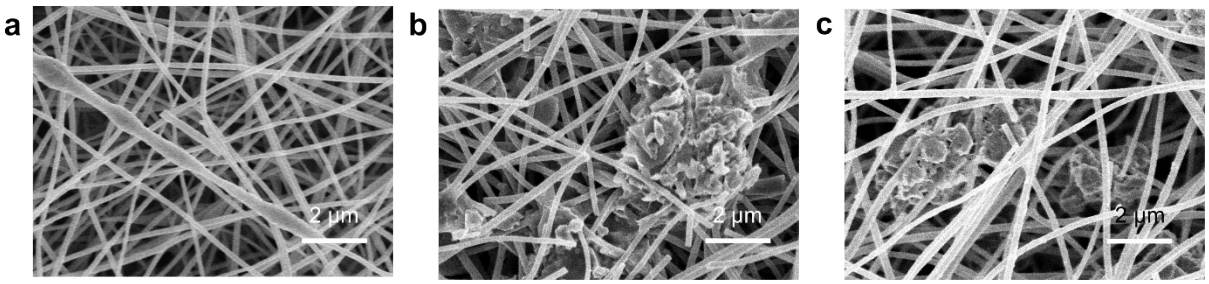

Fig. S40 SEM images of (a) a fresh, (b) a discharged and (c) a recharged MnTA/PAN-800 cathode tested under 0.04 mA cm^{-2} with a cut-off capacity of 1.0 mA h cm^{-2}.

Table S1. Surface areas and pore volumes of different electropsun nanofibers.

	S_{BET} (m^2 g^{-1})	V_{total} (cm^3 g^{-1})	V_{meso} (cm^3 g^{-1})
PAN-800	958	0.49	0.10
Mn/PAN-800	39	0.12	0.10
MnTA/PAN-800	133	0.12	0.06
MnO@NMCNF-600	113	0.53	0.48
MnO@NMCNF-700	105	0.53	0.49
MnO@NMCNF	101	0.59	0.55
MnO@NMCNF-900	178	0.87	0.80

Table S2. R_s and R_{ct} values of different fresh Mn(II)-based electrodes.

	R_s	R_{ct}
MnO@NMCNF-600	31.68	177.8
MnO@NMCNF-700	37.01	145.2
MnO@NMCNF	28.79	55.84
Mn/PAN-800	27.68	471.8
MnTA/PAN-800	26.5	413.7

Table S3. Element contents of different freestanding electrodes using elemental analysis or ICP-OES.

	Content from elemental analysis (wt%)		Content from ICP (wt%)
	C	N	Mn
PAN-800	91.2	5.2	N/A
Mn/PAN-800	29.4	3.8	48.9
MnTA/PAN-800	33.6	4.7	41.4
MnO@NMCNF	27.3	7.6	38.5

Table S4. Performance of existing Li–CO_2 cells working in pure CO_2.

	Areal capacity (mA h cm^{-2})	Electrode capacity (mA h g^{-1}) [a]	Cut-off voltage (V)	Cycling performance (cut-off capacity, mA h cm^{-2}/current, mA cm^{-2}/ cycle number)	Substrate	Ref.
MnO@ NMCNF	**19.07**	**8668**	**2.0**	**1/0.08/52**	**freestanding**	**This work**
Graphene	4.7	553	2.2	0.5/0.025/20	carbon paper	[1]
CNT	2.68	316	2.2	0.5/0.025/29	carbon paper	[2]
B,N-codoped holey graphene	4.81	567	2.0	0.3/0.3/200	carbon paper	[3]
CQD/hG	1.23	149	2.0	0.05/0.1/235	carbon paper	[4]
Ru/Ni foam	1.36	40	2.0	0.15/0.03/100	Ni foam	[5]
Ru@Super P	2.47	291	2.0	0.3/0.09/70	carbon paper	[6]
RuO_2/CNT	0.87	102	2.2	0.2/0.02/55	carbon paper	[7]
RuO_2/LDO	1.36	40	2.5	0.25/0.04/60	Ni foam	[8]
Ru-Cu NPs/G	3.84	454	2.3	0.28/0.1/100	carbon paper	[9]
RuP_2/NPCF	2.39	286	2.0	0.2/0.04/200	carbon paper	[10]
Ru/ACNFs	4.6	11495	2.0	0.4/0.04/50	**freestanding**	[11]
Ru/CNT/ Wood	11	1.25	2.0	0.28/0.0.05/200	**freestanding**	[12]
Ir/C NF	11.54	N/A	2.0	0.1/0.02/120	**freestanding**	[13]
IrO_2/MnO_2	2.64	184	2.0	1/0.4/378	carbon cloth	[14]

Ir NSs-CNFs	2.3	272	2.0	0.3/0.15/400	carbon paper	[15]
NiFe@NC/PPC	6.8	518	2.0	0.25/0.05/109	**freestanding**	[16]
P-Mn_2O_3	7.55	841	2.0	0.8/0.04/50	carbon paper	[17]
Mo_2C/CNT	0.75	73	2.0	0.06/0.01/40	carbon paper	[18]
Ni-NG	5.64	664	2.2	0.32/0.03/101	carbon paper	[19]
Ni/rGO framework	14.6	8991	2.0	1.62/0.16/100	**freestanding**	[20]
Cu-NG	4.76	560	2.2	0.32/0.12/50	carbon paper	[21]
ZnS NST/N-rGO	3.3	389	2.0	0.32/0.13/190	carbon paper	[22]
CoPPc	13.6	909	2.0	1/0.05/50	carbon cloth	[23]
Mn-MOF	5.77	679	2.0	0.32/0.06/50	carbon paper	[24]
MnO@NC-rGO	8	943	2.0	0.32/0.32/200	carbon paper	[25]

[a] Electrode capacity is calculated based on the total mass of substrate and catalyst in the cathode side.

References

[1] Z. Zhang, Q. Zhang, Y. Chen, J. Bao, X. Zhou, Z. Xie, J. Wei and Z. Zhou, *Angew. Chem. Int. Ed.*, 2015, **54**, 6550-6553.

[2] X. Zhang, Q. Zhang, Z. Zhang, Y. Chen, Z. Xie, J. Wei and Z. Zhou, *Chem. Commun.*, 2015, **51**, 14636-14639.

[3] L. Qie, Y. Lin, J. W. Connell, J. Xu and L. Dai, *Angew. Chem. Int. Ed.*, 2017, **56**, 6970-6974.

[4] Y. Jin, C. Hu, Q. Dai, Y. Xiao, Y. Lin, J. W. Connell, F. Chen and L. Dai, *Adv. Funct. Mater.*, 2018, **28**, 1804630.

[5] H. Zhao, D. Li, H. Li, A. G. Tamirat, X. Song, Z. Zhang, Y. Wang, Z. Guo, L. Wang and S. Feng, *Electrochim. Acta*, 2019, **299**, 592-599.

[6] S. Yang, Y. Qiao, P. He, Y. Liu, Z. Cheng, J.-j. Zhu and H. Zhou, *Energy Environ. Sci.*, 2017, **10**, 972-978.

[7] S. Bie, M. Du, W. He, H. Zhang, Z. Yu, J. Liu, M. Liu, W. Yan, L. Zhou and Z. Zou, *ACS Appl. Mater. Interfaces*, 2019, **11**, 5146.

[8] S.-M. Xu, Z.-C. Ren, X. Liu, X. Liang, K.-X. Wang and J.-S. Chen, *Energy Storage Mater.*, 2018, **15**, 291-298.

[9] Z. Zhang, C. Yang, S. Wu, A. Wang, L. Zhao, D. Zhai, B. Ren, K. Cao and Z. Zhou, *Adv. Energy Mater.*, 2019, **9**, 1802805.

[10] Z. Guo, J. Li, H. Qi, X. Sun, H. Li, A. G. Tamirat, J. Liu, Y. Wang and L. Wang, *Small*, 2019, **15**, 1803246.

[11] Y. Qiao, S. Xu, Y. Liu, J. Dai, H. Xie, Y. Yao, X. Mu, C. Chen, D. J. Kline, E. M. Hitz, B. Liu, J. Song, P. He, M. R. Zachariah and L. Hu, *Energy Environ. Sci.*, 2019, **12**, 1100-1107.

[12] S. Xu, C. Chen, Y. Kuang, J. Song, W. Gan, B. Liu, E. M. Hitz, J. W. Connell, Y. Lin and L. Hu, *Energy Environ. Sci.*, 2018, **11**, 3231-3237.

[13] C. Wang, Q. Zhang, X. Zhang, X. G. Wang, Z. Xie and Z. Zhou, *Small*, 2018, **14**, 1800641..

[14] Y. Mao, C. Tang, Z. Tang, J. Xie, Z. Chen, J. Tu, G. Cao and X. Zhao, *Energy Storage Mater.*, 2019, **18**, 405-413.

[15] Y. Xing, Y. Yang, D. Li, M. Luo, N. Chen, Y. Ye, J. Qian, L. Li, D. Yang, F. Wu, R. Chen and S. Guo, *Adv. Mater.*, 2018, **30**, 1803124.

[16] H. Liang, Y. Zhang, F. Chen, S. Jing, S. Yin and P. Tsiakaras, *Appl. Catal. B Environ.*, 2019, **244**, 559-567.

[17] W. Ma, S. Lu, X. Lei, X. Liu and Y. Ding, *J. Mater. Chem. A*, 2018, **6**, 20829-20835.

[18] Y. Hou, J. Wang, L. Liu, Y. Liu, S. Chou, D. Shi, H. Liu, Y. Wu, W. Zhang and J. Chen, *Adv. Funct. Mater.*, 2017, **27**, 1700564.

[19] Z. Zhang, X. G. Wang, X. Zhang, Z. Xie, Y. N. Chen, L. Ma, Z. Peng and Z. Zhou, *Adv. Sci.*, 2018, **5**, 1700567.

[20] Y. Qiao, Y. Liu, C. Chen, H. Xie, Y. Yao, S. He, W. Ping, B. Liu and L. Hu, *Adv. Funct. Mater.*, 2018, **28**, 1805899.

[21] Z. Zhang, Z. W. Zhang, P. F. Liu, Y. P. Xie, K. Z. Cao and Z. Zhou, *J. Mater. Chem. A*, 2018, **6**, 3218-3223.

[22] H. Wang, K. Xie, Y. You, Q. Hou, K. Zhang, N. Li, W. Yu, K. P. Loh, C. Shen and B. Wei, *Adv. Energy Mater.*, 2019, **9**, 1901806.

[23] J. Chen, K. Zou, P. Ding, J. Deng, C. Zha, Y. Hu, X. Zhao, J. Wu, J. Fan and Y. Li, *Adv. Mater.*, 2019, **31**, 1805484.

[24] S. Li, Y. Dong, J. Zhou, Y. Liu, J. Wang, X. Gao, Y. Han, P. Qi and B. Wang, *Energy Environ. Sci.*, 2018, **11**, 1318-1325.

[25] S. Li, Y. Liu, J. Zhou, S. Hong, Y. Dong, J. Wang, X. Gao, P. Qi, Y. Han and B. Wang, *Energy Environ. Sci.*, 2019, **12**, 1046-1054.